Dhaka Univ. J. Sci. 73(2): 119-126, 2025 (July)
ISSN 1022 - 2502, E-ISSN 2408-8528
DOI: https://doi.org/10.3329.dujs.v73i2.82770

# Numerical Analysis of Turbulent Flow through a Ducted Propeller

**Md. Zavid Iqbal Bangalee*, Tausif Ahmed, and Kajal Chandra Saha**
*Department of Applied Mathematics, University of Dhaka, Bangladesh*
(Received: 20 December 2023; Accepted: 8 April 2025)

## Abstract

The current world of air travel has become significantly option-heavy over the past few decades. There are commercial jet-liners, helicopters, and private jets. In all these advancements in air travel, one aspect has always been of significant importance: ducted-propelled aircraft. A duct, though simple in form, can lead to an increase in the efficiency of an aircraft. The position of the duct, its thickness, its radius, and the material it has been made of all play essential roles in nominating a certain duct for a specific aircraft. In this study, the numerical analysis of turbulent flow through a ducted propeller will be observed, and different aerodynamic coefficients will be computed. This study will show that a ducted propeller is capable of producing significant lift for an automatic or manual aircraft to fly through turbulence.

***Keywords***: Turbulent flow, Duct, Propeller, UAV

## I. Introduction

Throughout the early 20th century, researchers and engineers made significant advances in propeller design, considering factors like blade shape, pitch, and material. To increase propulsion efficiency and decrease energy losses, scientists and engineers improved the size and design of the ducts. The initial significant practical investigation into ducted propellers seems to have been made public in Italy in 1931 by Luigi Stipa[1]. Stipa conducted methodical experiments within a wind tunnel, which distinctly revealed the advantages of enclosing or covering the propeller when stationary. Since then numerous people, companies, academic institutions, and government organizations, both domestic and international, have participated in providing input for the survey. In reality, the design and analysis of a ducted propeller is quite challenging as it contains all the difficulties associated with the design of open propellers[2]. When analyzing open propellers, a researcher has options to choose from and methods to consider. On the other hand, analyzing a ducted propeller calls for observing at least two solid bodies, the propeller, and the duct. Rigorous research has been carried out by Naldi et al.[3] in the field of analyzing and implementing ducted propellers in modular air robots. According to the suitable selection of interconnection topology, the recommended category of vehicles can display a variety of dynamic behaviors, ranging from underactuated to fully actuated. Another impactful work was done by David et al.[4] where a small robot called FCSTAR was observed to fly and crawl over or beneath possible obstructions. This robot was developed using ducted propeller technology. Throughout recent aerospace history, the use of ducted propellers has become something of great importance. Besides implementation in aerial vehicles, a lot of autonomous underwater vehicles (AUVs) are making use of ducted propellers[5]. One of the reasons for using ducted propellers rather than open-rotor propellers[6] is that it decreases the noise generated by a sea vessel, which is something highly desirable. Another important study was carried out by Gong et al.[7] which shed light on blade-blade interference and blade-duct interaction through various configurations between ducted and non-ducted propellers. The observation indicates that the interaction between blades, known as blade-blade interference, contributes positively to loading stability. Additionally, the presence of a duct accelerates the decrease in efficiency as the number of blades increases in a single-blade configuration.

The Bell XV-3 was one of the first American attempts at a tilt-rotor aircraft and was created as an investigation of convertiplane technology[8]. Convertiplanes were distinguished from modern helicopters by their capacity to execute vertical takeoff and landing (VTOL) while traveling at higher speeds in forward flight. The aircraft, built in 1955, had two wing-mounted proprotors that could change the plane of rotation of the craft by 90°, allowing it to quickly go from a vertical upward posture for takeoff and landing to a position facing forward for forward flight. A Pratt and Whitney R-985-AN-1 radial reciprocating engine supplied power to the outboard rotors via shafts. The rotor rotation of xv-3 combined the benefits of both flight modes, allowing it to hover like a helicopter and reach high forward speeds like an airplane. The Hiller X-18 was a different tiltrotor technology experiment, making it a vertical/short takeoff and landing (V/STOL) aircraft because of its ability to roll during short takeoffs. Instead of simply tilting the rotors or using large propellers, the X-18[8] offered a novel strategy by additionally tilting its large wing. With this wing modification, lift could be produced at faster airspeeds. The huge planform area of the wing served as a sail in its vertical lift mode, making the airplane susceptible to unmanageable situations brought on by unexpected wind gusts. This restriction required the employment of a different craft design without large tilting wings. In another study, Zhang et al.[9] observed the wake dynamics of a ducted propeller numerically. According to this work, a new and unique understanding is offered regarding the

* Author for correspondence. e-mail : zavid@du.ac.bd

instability mechanism connected to the disruption of the tip leakage vortex within the wake of a ducted propeller. Applications including Personal Air Vehicles (PAVs), drones, and helicopter tail rotors are good fits for this technology[10,11] When compared to an open propeller, the ducted propeller demonstrates greater aerodynamic efficiency, principally because the duct can produce more thrust with the same power input[12]. In recent time, Hu et al.[13] have done outstanding work in the field of hovering efficiency optimization. Over all, substantial research efforts have been focused on improving the duct's geometry. According to Taylor's experimental studies of ducted propellers in hovering situations, reducing the lip radius increases the efficiency of static thrust and duct thrust.

## II. Mathematical Model

**$K-\varepsilon$ Two Equation Model:** This is the most used two-equation eddy-viscosity model [14]. As evident from its name, this model is based on the solution of turbulent kinetic energy ($K$) and turbulent dissipation rate ($\varepsilon$). This model was introduced by Chou [15]. During the early 80s, different formulations of the model were proposed which in consequence paved the way for today's model.$K-\varepsilon$models correspond to high Re whereas $K-\omega$ models are mostly low Re models. That is why a $K-\varepsilon$ RANS model is used in this study.

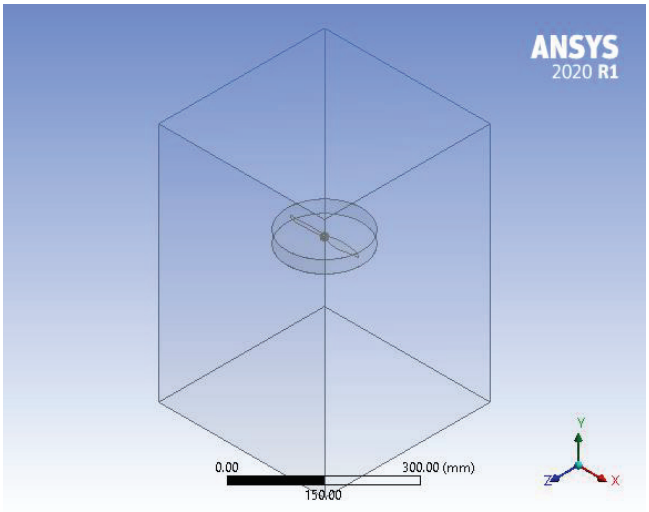


**Fig. 1.** Boundary region around the primary geometry.

### *Differential Form*

A low Reynolds number $K-\varepsilon$ model can be written as

$$\frac{\partial \rho K}{\partial t}+\frac{\partial}{\partial x_j}\left(\rho v_j K\right) = \frac{\partial}{\partial x_j}\left[\left(\mu_L+\frac{\mu_T}{\sigma_K}\right)\frac{\partial K}{\partial x_j}\right]+\tau_{ij}^{F}S_{ij} - \rho\varepsilon \tag{1}$$

$$\frac{\partial \rho \varepsilon^*}{\partial t}+\frac{\partial}{\partial x_j}\left(\rho v_j \varepsilon^*\right) = \frac{\partial}{\partial x_j}\left[\left(\mu_L+\frac{\mu_T}{\sigma_\varepsilon}\right)\frac{\partial \varepsilon^*}{\partial x_j}\right] + C_{\varepsilon 1}f_{\varepsilon 1}\frac{\varepsilon^*}{K}\tau_{ij}^{F}S_{ij} - C_{\varepsilon 2}f_{\varepsilon 2}\rho\frac{(\varepsilon^*)^2}{K}+\varphi_\varepsilon \tag{2}$$

The terms on the right-hand side are conservative diffusion, eddy-viscosity production, and dissipation. Moreover, $\varphi_\varepsilon$ denotes the explicit wall term. Here the term $\mu$ is given by

$$\mu=\mu_L+\mu_T \tag{3}$$

where $\mu_L$ and $\mu_T$ are laminar and turbulent viscosity components respectively.

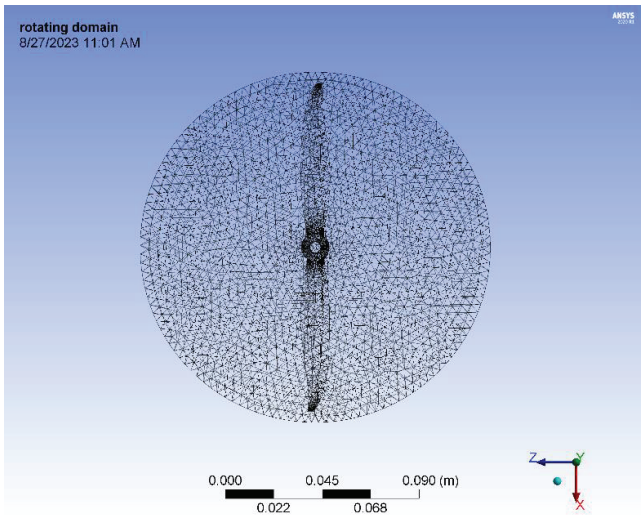


**Fig. 2.** Meshing of the rotating domain.

Again,

$$\mu_T=C_\mu f_\mu \rho\frac{K^2}{\varepsilon^*} \tag{4}$$

The quantity $\varepsilon^*$ has a relationship with the turbulent dissipation rate $\varepsilon$ by

$$\varepsilon=\varepsilon_w+\varepsilon^* \tag{5}$$

Here, $\varepsilon_w$ is the value of the dissipation rate at the wall. The other constants and the turbulent Prandtl number are given below.

$C_\mu=0.09,\ C_{\varepsilon 1}=1.44,\ C_{\varepsilon 2}=1.92,\ \sigma_K=1.0,\ \sigma_\varepsilon=1.3,$ $Pr_T=0.9.$

Additionally, the near-wall damping functions are

$$f_\mu=e^{\left(\frac{-3.4}{(1+0.02Re_T)^2}\right)}$$
$$f_{\varepsilon 1}=1 \tag{6}$$
$$f_{\varepsilon 2}=1-0.3e^{Re^2{}_T}$$

with $Re_T = \rho K^2/(\varepsilon^* \mu_L)$ being the turbulent Reynolds number. In the end, the explicit wall term $\varphi_\varepsilon$ and $\varepsilon_w$ are defined as

$$\varphi_\varepsilon = 2\mu_T \frac{\mu_L}{\rho}\left(\frac{\partial^2 v_s}{\partial \gamma_n{}^2}\right)^2 \text{ and } \varepsilon_w = \frac{2\mu_L}{\rho}\left(\frac{\partial \sqrt{K}}{\partial \gamma_n}\right)^2 \quad (7)$$

where $v_s$= velocity parallel to the wall, and $\gamma_n$= coordinate normal to the wall. To avoid an explicit knowledge of the wall distance and orientation, it is common to calculate the wall term and $\varepsilon_w$ from the following Cartesian tensor form

$$\varphi_\varepsilon = 2\mu_T \frac{\mu_L}{\rho}\left(\frac{\partial^2 v_i}{\partial x_j \partial x_k}\right)^2 \text{ and } \varepsilon_w = \frac{2\mu_L}{\rho}\left(\frac{\partial \sqrt{K}}{\partial x_j}\right)^2 \quad (8)$$

instead of Eq. (7).

## III. Generation of Mesh and Boundary Conditions

The fluid domain has been constructed keeping in mind that the walls of the domain do not in any way affect the flow around the main body. Meshing has been done in ANSYS Mesh software.

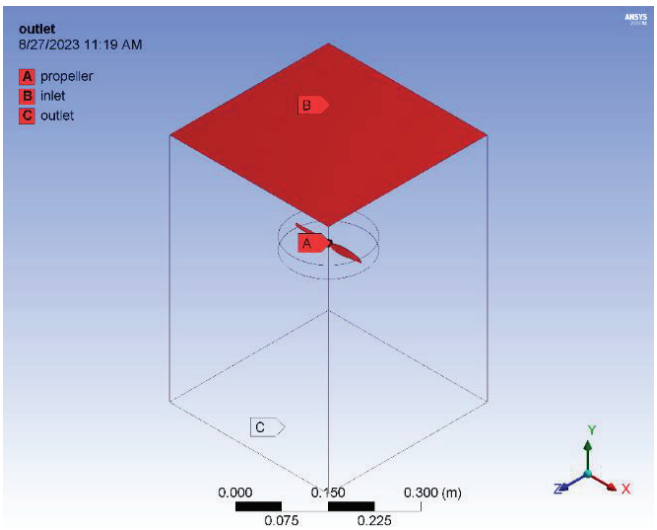


**Fig. 3.** Inlet, outlet, and propeller.

The propeller has been meshed initially, trailed by the duct. Once the meshing of the rotating domain has been done, the last part which is meshing the static domain is left. The static domain is generated by implementing a properly sized enclosure around the rotating domain. Meshing information of the ducted propeller has been shown in the following table. To capture the flow behavior as accurately as possible, the total elements number has been set to 1.4 million(approximately).

**Table 1. Mesh Report**

| Domain | Nodes | Elements |
|---|---|---|
| Rotating Domain | 44155 | 236556 |
| Static Domain | 201040 | 1145336 |
| All Domains | 245195 | 1381892 |

## IV. Characteristics of the Flow

A turbulent flow [16] is directed through the ducted propeller, and its characteristics are observed. According to Newman [17], the efficiency of a propeller can be increased by using an actuator disk. However, in the current study, the focus will be on the efficiency of a simpler duct around the main body of the propeller. In the following table, the data on flow specifications are provided.

## V. Numerical Method

To solve the system numerically, ANSYS Fluent uses the fluent solver software. It is a high-accuracy solver that numerically interpolates the initial solution to find the final solution. At the same time, this solver makes sure that the solution is converging and not diverging. The calculation is done over a pre-set number of time steps. More iterations or steps result in a better convergence criterion. The two equation $K-\varepsilon$ model is used in this solution with 100 time steps each sized 0.00015 seconds. The maximum number of iterations is set to 15 with both reporting and profile update intervals set to 1. The following table shows the reference values for this solution.

**Table 2. Reference Values**

| | |
|---|---|
| **Area ($m^2$)** | 1 |
| **Density ($kg/m^3$)** | 1.225 |
| **Enthalpy (J/kg)** | 0 |
| **Length (m)** | 1 |
| **Pressure ($N/m^2$)** | 0 |
| **Temperature (K)** | 288.16 |
| **Velocity (m/s)** | 1 |
| **Viscosity (kg/m-s)** | $1.7894 \times 10^{-5}$ |
| **Ratio of Specific Heats** | 1.4 |

## VI. Convergence Conditions

For the current study, the convergence conditions have been set using the residual monitors of ANSYS Fluent. Here, the absolute criteria for continuity has been set to $10^{-3}$. Only the convergence of continuity will be checked because if the numerical solution ends up being a continuous one then all the other parameters will converge. The convergence criterion is a way for the solution to eliminate nonlinearities to ensure the final run. For different angular velocities, the residual graphs will change.

## VII. Results

After mesh has been generated, the setup software of ANSYS Fluent is used to set up the system. Once the calculation is run properly, ANSYS Solver will provide a residual graph, and a thrust force graph. Furthermore, pressure and velocity contours will be presented. The residual graph for angular velocities 6000, 8000, and 10000 rpm are shown below. In

the following figures, a range of iterations from 0-1800 has been used. To get as close as possible to the experimental results without sacrificing too much computational resources, the following ranges have been chosen for the parameters.

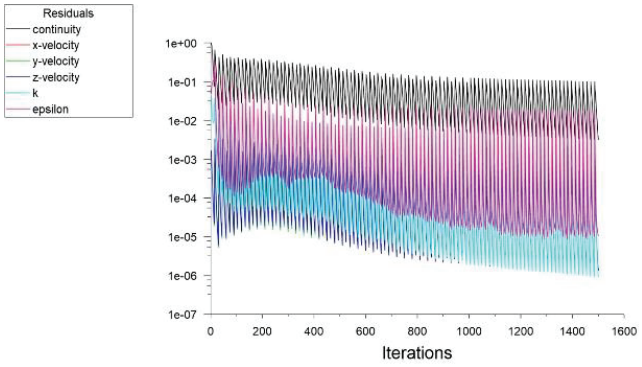


**Fig. 4.** Residual Graph for RPM=6000.

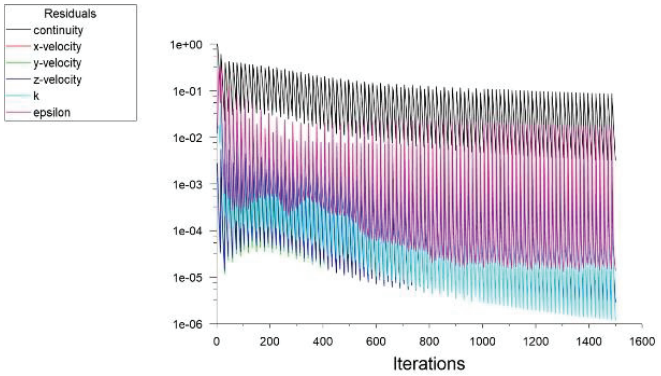


**Fig. 5.** Residual Graph for RPM=8000.

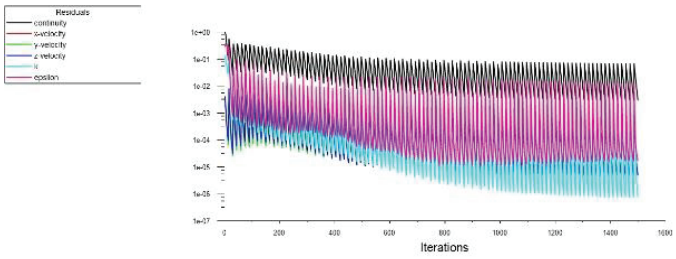


**Fig. 6.** Residual Graph for RPM=10000.

The main force working to keep the aircraft flying is the thrust force. In this study, thrust force is calculated against flow time in seconds. Below the convergence graphs of the thrust force are shown.

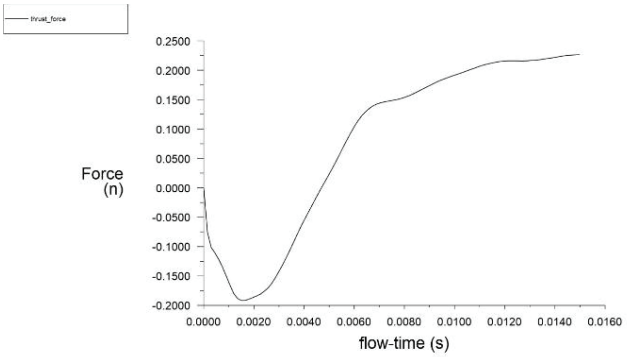


**Fig. 7.** Thrust Force for RPM=6000.

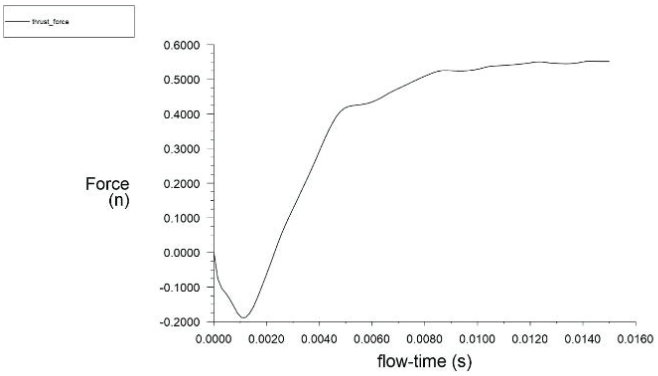


**Fig. 8**. Thrust Force for RPM=8000.

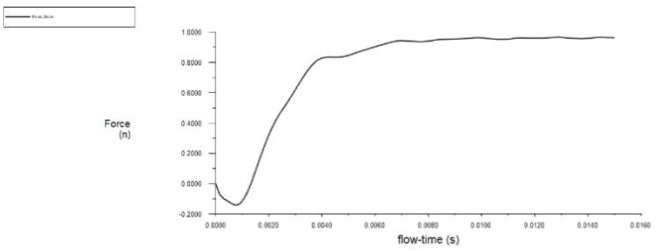


**Fig.** 9. Thrust Force for RPM=10000.

It is evident from the graphs above that as angular velocity (RPM) is increased, the thrust force also increases, and their convergence characteristics become more accurate. Due to an increase in rotation per minute, the cumulative force rises. To put things into perspective, the following table depicts the relationship between angular velocity and thrust force.

**Table 3. Relationship between Angular Velocity and Thrust Force**

| RPM | Thrust Force (N) |
|---|---|
| 6000 | 0.36948567 |
| 8000 | 0.76885393 |
| 10000 | 1.4176027 |

## VIII. Contours

The velocity and pressure gradients print a better picture of the behavior of the flow through the ducted propeller. The contours for RPM 6000, 8000 and 10000 are given below.

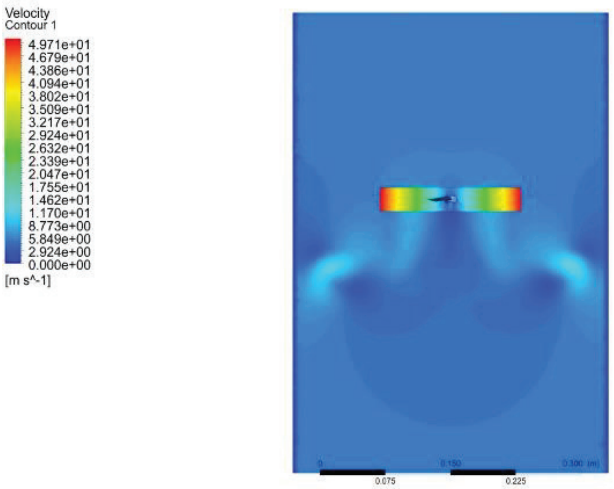


**Fig. 10.** Velocity Contour for RPM=6000.

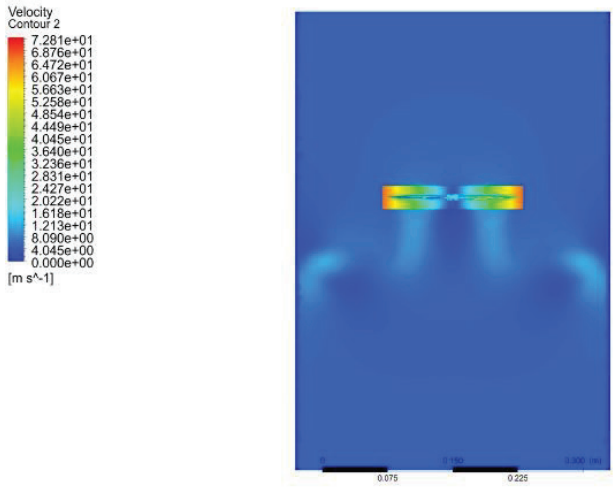


**Fig. 11.** Velocity Contour for RPM=8000.

From the figures, it is evident that for all three angular velocities, vortices form around the bottom left and right corners of the ducted propeller. The shape of the vortices gradually changes because they have open particle paths. This results in a moving vortex. When two or more vortices are close together, they merge to make a single vortex.

The pressure contours depict the fluctuations in pressure resulting from varying angular velocities. Pressure contours corresponding to three different angular velocities are displayed below.

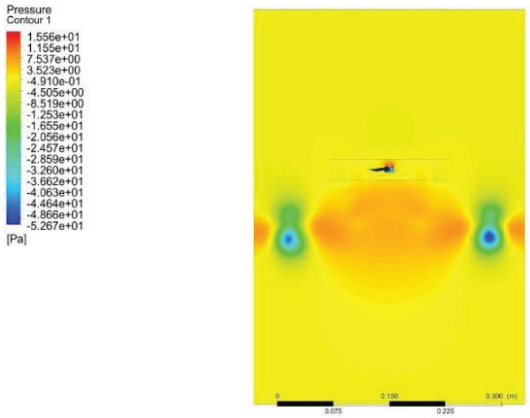


**Fig. 12.** Pressure Contour for RPM=6000.

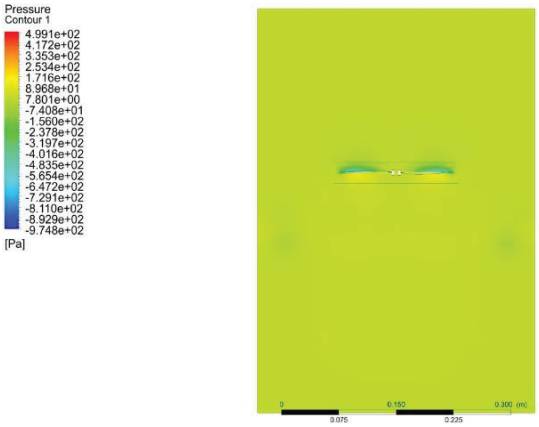


**Fig. 13.** Pressure Contour for RPM=8000.

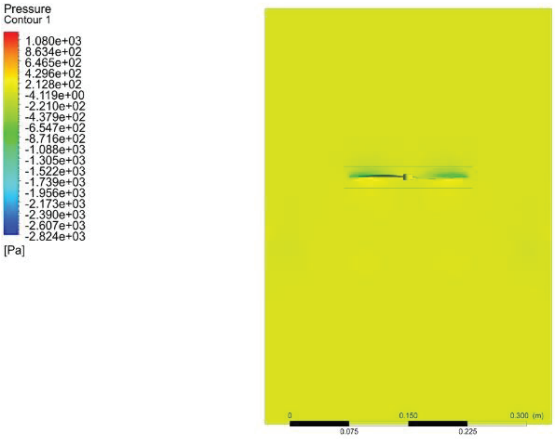


**Fig. 14.** Pressure Contour for RPM=10000.

The streamlines are another measure for observing the behavior of the flow through the ducted propeller. Streamlines at 6000, 8000 and 10000 RPM are shown below.

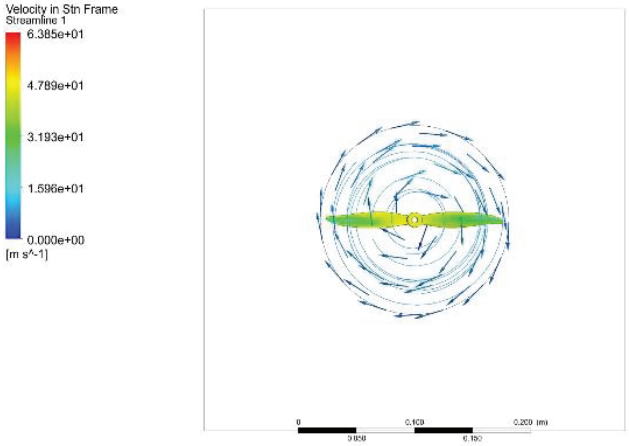


**Fig. 15.** Streamlines at RPM=8000 for N=50.

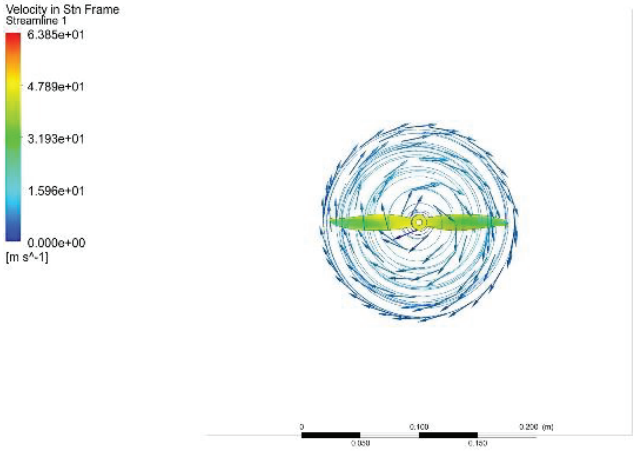


**Fig. 16.** Streamlines at RPM=8000 for N=100.

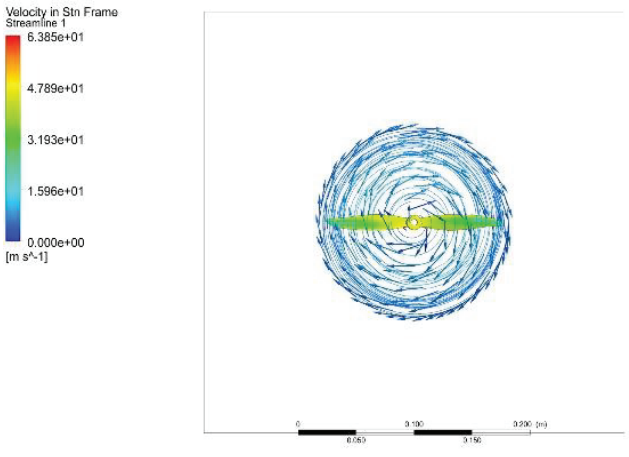


**Fig. 17.** Streamlines at RPM=8000 for N=150.

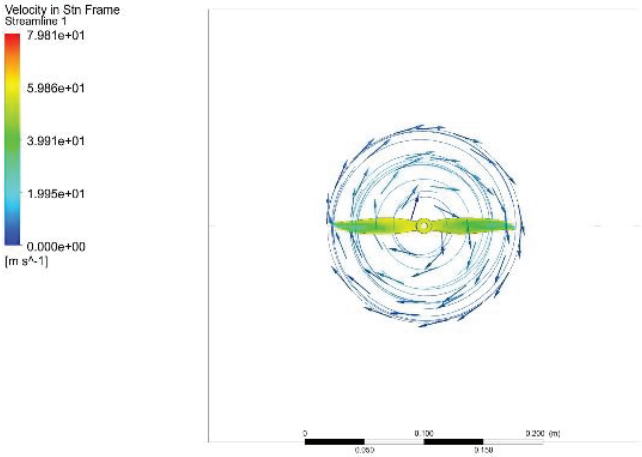


**Fig. 18.** Streamlines at RPM=10000 for N=50.

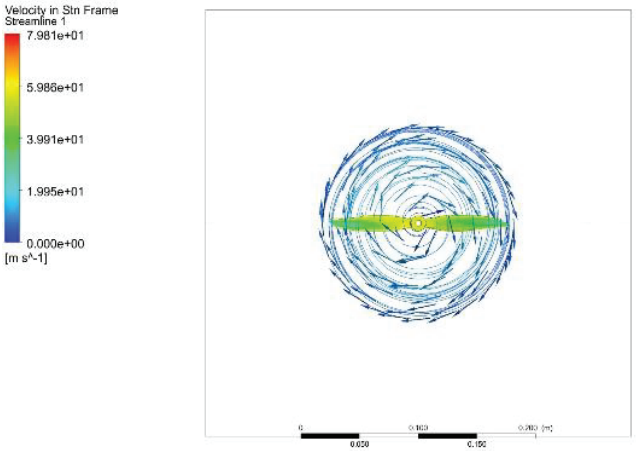


**Fig. 19.** Streamlines at RPM=10000 for N=100.

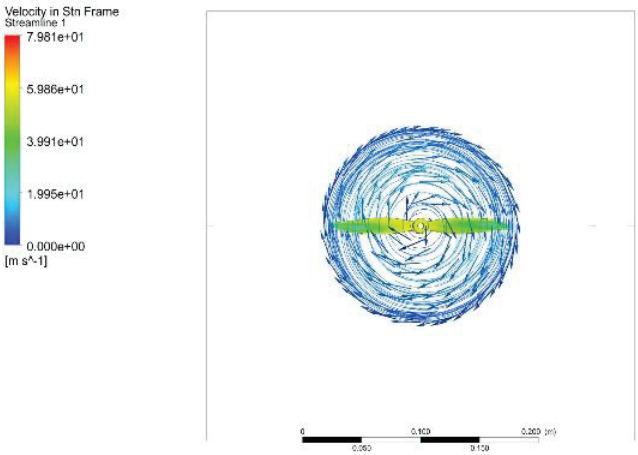


**Fig. 20.** Streamlines at RPM=10000 for N=150.

It is evident from the figures that as the angular velocity is increased, the streamlines become more tangential to the direction of the blade. It occurs due to an increasing angular momentum. Below is another perspective of the streamlines at RPM= 10000.

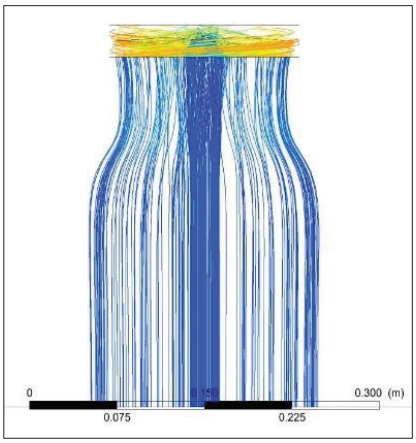


**Fig. 21.** Streamlines view from XY-plane.

Inside the rotating domain, the streamlines go through a significant fluctuation which is characterized by a varying velocity.

## IX. Conclusions

The current study sheds light on several important aspects, which are given below.

1. The implementation of a duct increases the efficiency of a propeller.
2. An increase in the angular velocity increases the thrust force of the aircraft.
3. Vortices are generated around the rear side of the ducted propeller due to the open particle paths.
4. The angular velocity cannot be increased because it will result in inconsistent thrust force.
5. The streamlines around the propeller become more tangential as the angular velocity is raised.
6. For angular velocity less than RPM= 2000 the thrust force cannot remain positive, which means that even though the aircraft takes flight, it cannot stay in the air for long.
7. The thrust force highly depends on the shape and size of the duct.

Many studies have already been done on different types of propellers. However, the aim of the current work was to observe the behavior of turbulent flow through a duct. The results of this work will help future researchers to fine-tune the differences between a ducted and a ductless propeller which, in time, may pave the way towards various automatic aircrafts such as UAM, eVTOL etc. To summarize it can be said that an aircraft that has ducted propellers can produce a significantly better thrust force compared to a ductless propeller. However, if the placement of the duct is not accurate, it may not affect the thrust force at all. Therefore, to ensure a proper thrust force, it is a must to make sure that the position of the duct is accurate and that the aircraft is flying at the optimal angular velocity.

## Acknowledgement

Authors are highly grateful to Centennial Research Grant (2nd Phase), University of Dhaka and the University Grants Commission of Bangladesh for providing the financial support. Authors also acknowledge the facilities provided by the Department of Applied Mathematics, University of Dhaka.

## References

1. Sacks, A. H., J. A., Burnell, 1962, "Ducted Propellers—a Critical Review of the State of the Art", *Progress in Aeronautical Sciences*, **3**, 85-135
2. Kerwin, J. E., S. A., Kinnas, J., Lee, W., Shih, 1987, "A Surface Panel Method for the Hydrodynamic Analysis of Ducted Propellers", *The Society of Naval Architectures and Marine Engineers*, **4**, 1-22
3. Naldi, R., F., Forte, A., Serrani, L., Marconi, 2015, "Modeling and Control of a Class of Modular Aerial Robots Combining Under Actuated and Fully Actuated Behavior", *IEEE Transactions on Control Systems Technology*, **23(5)**, 1869-1885
4. David, N. B., D., Zarrouk, 2021, Design and Analysis of FCSTAR, a Hybrid Flying and Climbing Sprawl Tuned Robot, *IEEE Robotics and Automation Letters*, **6(4)**, 6188-6195
5. Zimmerman, R., D'Spain, G. L, D. C., Chadwell, 2005, "Decreasing the Radiated Acoustic and Vibration Noise of a Mid-Size AUV", *IEEE Journal of Oceanic Engineering*, **30**, 179-187
6. Grinyok, A., Boychuk, I., D., Perelygin, I., Dantsevich, 2018, "Simulation in Production of Open Rotor Propellers: From Optimal Surface Geometry to Automated Control of Mechanical Treatment", *IOP Conference Series: Materials Science and Engineering*, **327**, 1-6
7. Gong, J., Ding, J., Wang, L., 2021, Propeller–duct Interaction on the Wake Dynamics of a Ducted Propeller, *Physics of Fluids*, **33**, 1-13
8. Wilroy, J. A., 2021, Tilt-rotor Ducted Fans and their Applications, *Aerospace Engineering,* **23**, 89-101
9. Zhang, Q., R. K., Jaiman, 2019, "Numerical Analysis on the Wake Dynamics of a Ducted Propeller", *Ocean Engineering*, **171**, 202-224
10. Rostami, M., A., Farajollahi, 2021, "Aerodynamic Performance of Mutual Interaction Tandem Propellers with Ducted UAV",*Aerospace Science and Technology*, **108**, 1-15
11. Deng, S., Wang, S, Zheng, Z., 2020, "Aerodynamic performance assessment of a ducted fan UAV for VTOL applications", *Aerospace Science and Technology*, **103**, 1-32
12. Yilmaz, S., Erdem, D., Kavsaoglu, M.S., 2015, "Performance of a Ducted Propeller Designed for UAV Applications at Zero Angle of Attack Flight: An Experimental Study", *Aerospace Science and Technology*, **1(156)**, 1-11

13. Hu, Y., X. C., Zhang, G. Q., Yang, X. P., Xhang, Li, X. Z., 2024,"Hovering efficiency optimization of ducted propeller with large blade tip clearance based on grooved duct configuration", *Aerospace Science and Technology,* **150**, 109226

14. Blazek, J., 2015, "Chapter 7 – Turbulence Modeling", *Computational Fluid Dynamics: Principles and Applications*, 213-252

15. Chou, P. Y., 1945, On Velocity Correlations and the Solutions of the Equations of Turbulent Fluctuations", *Quarterly of Applied Mathematics*, **3**, 38-54

16. Gerolymos, G. A., Vallet, I., 1998, "Implicit Computation of Three-Dimensional Compressible Navier-Stokes Equations using $K-\varepsilon$ Closure", *AIAA Paper*, **97**-0430

17. Lakshminarayana, B., 1986, "Turbulence Modeling for Complex Shear Flows", *AIAA Journal*, **24**:1900-17